CrystEngComm

PAPER

View Article Online
View Journal | View Issue

Cite this: *CrystEngComm*, 2025, **27**, 507

Elucidating trends in synthesis and structural periodicity in a series of tetravalent actinide–oxo hexamers†

Thomas L. McCusker, [a] Nicole A. Vanagas, [a] Jennifer E. S. Szymanowski, [b] Robert G. Surbella III, [c] Jeffery A. Bertke, [a] Ana Arteaga *[c] and Karah E. Knope *[a]

Metal ion hydrolysis and condensation reactions are critical to describing the chemical behavior of the tetravalent actinides (An) due to their high charge density. This recognition has fueled synthetic efforts targeting polynuclear actinide–oxo clusters. Oligomers ranging from trimers to octatriacontamers have been reported, with the hexameric unit, which typically exhibits a $[An_6(OH)_4O_4]^{12+}$ core, representing the most pervasive cluster. Hexamers decorated by a range of ligands, including carboxylates, sulfates, and chlorides, have been described. Previous reports have demonstrated the formation of hexamers for Th, U, Np, and Pu both in solution and the solid state, yet little work has focused on the synthesis and properties of structurally analogous clusters across the early An series using the same complexing ligand. Here, a series of benzoate (Bz) decorated actinide–oxo/hydroxo hexamers of the same general formula $[An_6O_4(OH)_4(Bz)_{12}(H_2O)_n]$, where An = Th, U, Np, Pu and n = 6 for Th and 4 for U–Pu is reported. The title compounds were characterized by X-ray diffraction, UV-vis–NIR absorbance, Raman, and infrared spectroscopy. Notably isolation of these phases and elucidation of the parameters that underpin their formation provides insight into the ways differences in metal ion charge density manifest across the early tetravalent actinides, both in their synthetic and structural chemistry.

Received 11th October 2024,
Accepted 12th December 2024

DOI: 10.1039/d4ce01042f

rsc.li/crystengcomm

Introduction

The actinides have been the subject of research for decades, namely due to their application in nuclear energy and security; however, their radioactivity and limited abundance have caused our understanding of actinide (An) chemical behavior to lag behind that of the rest of the periodic table. Nonetheless, it has long been recognized that understanding the solution and solid-state speciation of the actinides is critically important to areas ranging from thermodynamics to waste management and environmental transport.[1]

The speciation of actinide elements is dependent on several factors, but is principally governed by oxidation state.[2,3] The early actinides, Th–Pu, adopt a common +4 oxidation state and the high charge density of the An^{4+} ions plays an integral role in describing the chemical behavior of the actinides in aqueous systems.[4] Specifically, tetravalent actinides tend to undergo hydrolysis in the presence of water.[2,5] The propensity of the An^{4+} ions to hydrolyze increases with increasing charge density, from Th^{4+} to Pu^{4+}, as a result of radial contraction brought on by poor shielding of the f-electrons.[6] Actinide–hydroxide products are formed as a result of hydrolysis, and these species undergo subsequent condensation reactions to yield oligomers,[2] either through oxolation or olation, which are characterized by the formation of oxo or hydroxo bridges, respectively. It is broadly recognized that these species are important to describing fundamental and applied aspects of actinide behavior[1,7–11] and have thus motivated investigations into the synthesis, characterization, and reactivity of actinide–oxo clusters.[2,12–14]

Tetravalent actinide–oxo clusters with nuclearities ranging from 3–38 have been described; the most prevalent structural unit is the hexanuclear cluster, with a $[An_6O_4(OH)_4]^{12+}$ core.[12–44] Synthetic parameters such as pH, temperature,

[a] *Department of Chemistry, Georgetown University, 37th and O Streets NW, Washington, D.C., 20057, USA. E-mail: tlm102@georgetown.edu, nv137@georgetown.edu, jb2667@georgetown.edu, kek44@georgetown.edu*
[b] *Department of Civil & Environmental Engineering & Earth Sciences, University of Notre Dame, 301 Stinson-Remick, Notre Dame, Indiana 46556, USA. E-mail: JSzymanowski@nd.edu*
[c] *Pacific Northwest National Laboratory, 902 Battelle Boulevard, Richland, WA 99354, USA. E-mail: robert.surbella@pnnl.gov, ana.arteaga@pnnl.gov*

† Electronic supplementary information (ESI) available: Crystallographic refinement details, thermal ellipsoid plots, powder X-ray diffraction patterns, and Raman spectra. Accession codes CCDC 2387949–2387951. For ESI and crystallographic data in CIF or other electronic format see DOI: **https://doi.org/10.1039/d4ce01042f**

solvent, and ligands influence the assembly of An^{4+}–oxo clusters.[27,29,30,45,46] Inorganic ligands, such as sulfate, nitrate, and chlorides, are effective in directing the formation of An^{4+}–oxo clusters. Moreover, hexamers capped by simple organic ligands with relevance to environmental systems, including glycine and formate, have also been reported.[21,43,47,48] While there is a growing catalog of An oligomers, few reports have focused on the synthesis and characterization of a series of clusters with the same capping ligand.[42] Such a series can be leveraged to understand trends in syntheses, which are reflective of the differences in metal ion acidity, and structural periodicity.

Here a family of tetravalent An^{4+}–oxo clusters (An = Th, U, Np, Pu) stabilized by benzoate capping ligands is described. The structures were determined by single crystal X-ray diffraction (SCXRD), and the vibrational properties were examined using infrared (IR) and Raman spectroscopy. Further, comparison of the ultraviolet-visible-near infrared (UV-vis–NIR) absorption spectra collected for the reaction solutions and solid-state allow identification of the clusters in solution. Differences in synthetic conditions and structural systematics across the series are observed and reflect the contraction in ionic radii, increasing charge density, and resulting hydrolysis and condensation behavior from Th–Pu.

Results and discussion

Synthesis

Reactions of $AnCl_4$ salts or $An^{4+}/HCl_{(aq)}$ solutions with benzoic acid (Bz) yielded four phases; **Th$_6$**, $[Th_6O_4(OH)_4(Bz)_{12}(H_2O)_6]$, **U$_6$**, $[U_6O_4(OH)_4(Bz)_{12}(H_2O)_4]\cdot 2(C_2H_6O)\cdot 2.5(H_2O)$, **Np$_6$**, $[Np_6O_4(OH)_4(Bz)_{12}(H_2O)_4]\cdot x(C_2H_6O)\cdot y(H_2O)$, and **Pu$_6$**, $[Pu_6O_4(OH)_4(Bz)_{12}(H_2O)_4]\cdot m(C_2H_6O)\cdot n(H_2O)$. These polynuclear species result from actinide hydrolysis and condensation reactions, and are important structural units for describing An behavior in aqueous systems.[3,16,18,49,50] Isolation of a series of structurally analogous hexamers, as reported here, and consideration of the variations in syntheses underscore differences in Brønsted acidity of metals ions. Moreover, spectroscopic investigations further inform the signatures that can be used for the detection and monitoring of stability of An^{4+}–oxo clusters.

The increase in metal ion charge density that occurs from Th^{4+} to Pu^{4+} is reflected in the propensity of these metal ions to hydrolyze and is evidenced in thermodynamic data. For example, the formation constants ($\log K$) for the first hydrolysis product, $M(OH)^{3+}$, for $Th(OH)^{3+}$, $U(OH)^{3+}$, $Np(OH)^{3+}$, and $Pu(OH)^{3+}$ are −2.500 ± 0.500, −0.540 ± 0.060, 0.550 ± 0.200, and 0.600 ± 0.200.[51,52] Tetravalent Th, with an ionic radius of 1.08 Å, is the largest of the An^{4+} and least likely to hydrolyze. The decreased susceptibility of Th to hydrolyze as compared to the other An^{4+} ions is evidenced in this work by observation of a non-hydrolyzed Th chain, $[Th(Bz)_4]_n$, which was previously reported by Falaise *et al.*[53] Notably, efforts to prepare the title compound, **Th$_6$**, by dissolution of $ThCl_4$ in H_2O/EtOH (ethanol) were unsuccessful irrespective of pH or metal to ligand ratio. The synthesis of the previously reported UiO-66 metal organic framework (MOF), a well reported MOF with a hexameric node of the general formula $[M_6O_4(OH)_4(C_8H_6O_4)_{12}]$, needed to be employed to target **Th$_6$**.[54] This allowed us to leverage water (which comes from the hydrated thorium chloride salt) as a reactant rather than a solvent, providing greater control over hydrolysis.

By comparison, **U$_6$**, **Np$_6$**, and **Pu$_6$** were synthesized from aqueous H_2O/EtOH solutions *via* slow evaporation (Table 1). For uranium, the second largest ion, slight differences in hydrolysis and condensation behavior are captured in the synthetic conditions such as pH and metal to ligand ratio. A much higher pH is required to isolate **U$_6$** than **Pu$_6$** and interestingly **Np$_6$** forms at a higher pH than **U$_6$**; however, six times as much benzoic acid is required for both **Np$_6$** and **Pu$_6$** to limit hydrolysis and direct the assembly of the hexamer. It should be mentioned that for **Pu$_6$**, this increase in the amount of benzoic acid could be necessary not only to thwart metal ion hydrolysis and condensation but also to offset the lower percentage of benzoic acid that is deprotonated at the lower pH of the Pu_6-solution. For reference, the pK_a of benzoic acid is 4.19. Ultimately, this study shows that while thorium and uranium are often used as surrogates for Np and Pu, under similar synthetic conditions they often demonstrate their own unique chemical behavior.

Structure descriptions

All members of the **An$_6$** series consist of $[An_6O_4(OH)_4(Bz)_{12}(H_2O)_n]$ (where An = Th, U, Np, Pu and n = 6 for Th and 4 for U, Np, Pu). A general description of these clusters is provided here, and further details in the ESI.† In each of the clusters, six An^{4+} metal centers are bridged through eight μ_3-oxygens to form a hexamer of composition, $[An_6O_4(OH)_4]^{12+}$. Twelve benzoate ligands decorate the cluster core, and a variable number of waters are bound directly to the actinide atoms.

Despite the similar core, there are several key differences between **Th$_6$** and the rest of the members of the **An$_6$** series. The **Th$_6$** compound consists of one unique Th coordination environment. The Th metal centers are 9-coordinate and adopt a monocapped square antiprism coordination geometry. Each Th is bound to one water molecule, four oxygens from four benzoates, and four μ_3-O/OH groups (Fig. 1). Conversely, the rest of the members of **An$_6$** exhibit metal centers with two unique coordination environments (Fig. 2). Like the Th counterpart, one of the metal centers is 9-coordinate and adopts a distorted monocapped square antiprismatic coordination geometry. The An is bound to a water molecule, four oxygen atoms from three benzoate molecules, two of which are monodentate bridging and one that is bidentate, and four μ_3-O/OH groups. The second metal is 8-coordinate and adopts a square antiprismatic coordination geometry with the metal bound to four μ_3-O/OH and four oxygen atoms from four monodentate bridging benzoates.

Table 1 Summary of synthetic conditions under which **Th$_6$**, **U$_6$**, **Np$_6$**, and **Pu$_6$** are formed

Phase	Solvent	Temperature	M : L ratio	pH
Th-chain	H_2O/EtOH	Room Temp. (immediate precipitation)	1 : 2–1 : 12	N/A
Th$_6$	DMF	130 °C	1 : 3.7	N/A
U$_6$	H_2O/EtOH	Room Temp. (slow evap.)	1 : 2	1.13
Np$_6$	H_2O/EtOH	Room Temp. (slow evap.)	1 : 12	2.28
Pu$_6$	H_2O/EtOH	Room Temp. (slow evap.)	1 : 12	0.64–1.01

Other structural differences are consistent with larger trends in periodicity in the actinide series. Most notably is the decrease in metal–oxygen bond lengths for An–μ_3-O/OH, An–O_{water}, and An–$O_{benzoate}$ from **Th$_6$** to **Pu$_6$**, (Table 2). The decrease in bond length from **Th$_6$** to **Pu$_6$** is consistent with the decrease in ionic radii from Th to Pu that arises from the actinide contraction. Another notable difference is reflected in the coordination environment from **Th$_6$** to **Pu$_6$**. The compound **Th$_6$** is entirely built from 9-coordinate metal centers while **U$_6$**–**Pu$_6$** exhibit both 8- and 9-coordinate metal centers.

Solution and solid-state UV-vis–NIR absorbance spectra

UV-vis–NIR absorption spectroscopy is a powerful technique for differentiating mononuclear and polynuclear An species.[23,24,42,45,46] As such, the solution and solid-state absorption spectra for **U$_6$**, **Np$_6$**, **Pu$_6$** were collected and compared to the An^{4+}/HCl stock solution. For **U$_6$** and **Np$_6$** the solution from which crystals precipitated was also analyzed.

The UCl_4 salt dissolved in 1 M HCl displays f–f transitions characteristic of U^{4+} (Fig. 3), with peaks observed at 495 nm, 549 nm, 648 nm, and 672 nm.[55] Notably, the spectrum of U^{4+} in 1 M HCl is consistent with that reported for U–H_2O–Cl species in aqueous solutions.[45] Upon the addition of benzoic acid in ethanol (**U$_6$**-solution), the peak centered at 663 nm increases in intensity relative to the peak centered at 648 nm. These bands are attributed to three transitions ($^3H_4 \rightarrow 3P_0$, $^3H_4 \rightarrow {}^1G_4$, and $^3H_4 \rightarrow {}^1D_2$), and previous work has shown the relationship between the higher wavelength (*i.e.*, 663 nm) and lower wavelength (648 nm) is diagnostic for the hexanuclear U^{4+}–oxo/hydroxo clusters in solution. The increased intensity of the 663 nm peak relative to the peak centered at 648 nm is consistent with the hexameric unit.[44,45] Interestingly, comparison of the **U$_6$**-crystals to solution shows notable differences, particularly between 600 nm and 700 nm; these differences have been observed in previously reported uranium hexamers and are attributed to differences in ligand binding and lattice solvent.[46]

The UV-vis–NIR absorption data of Np^{4+} in 1 M HCl, **Np$_6$**-solution, and **Np$_6$**-crystals are characteristic of Np^{4+} transitions with peaks at 590 nm, 730 nm, 820 nm, and 960 nm (Fig. 4).[56] Comparison of the Np^{4+} in 1 M HCl spectrum to that collected for the **Np$_6$**-solution shows a significant shift in the band centered at 730 nm to 740 nm. Such a red shift was also observed by Takao *et al.* and may be attributed to hexamer formation.[23] Also consistent with previous work is the growth in intensity of peaks at 604 nm and 899 nm in the **Np$_6$**-crystals spectrum relative to the Np solutions.[23] While the development of spectroscopic handles for neptunium-based clusters remains underdeveloped compared to uranium, this work further suggests spectral features may be diagnostic of neptunium oligomer formation and stability.

The UV-vis–NIR absorption spectra of Pu^{4+} in 1 M HCl and **Pu$_6$**-crystals are shown in Fig. 5. The Pu^{4+} stock solution spectrum exhibits peaks at 470 nm, 660 nm, 800 nm, and 1080 nm, all characteristic of Pu^{4+} in HCl.[57] Unfortunately, attempts to collect a UV-vis–NIR absorption spectrum of the **Pu$_6$**-solution were precluded by the low concentration of the plutonium. Nonetheless, comparison of the UV-vis–NIR absorption spectra of Pu^{4+} in 1 M HCl and **Pu$_6$**-crystals suggests a shift in the peak centered at ~470 nm to lower wavelengths (*i.e.*, 457 nm) (Fig. 5). The observed shift is diagnostic of Pu hexamers, as reported by Chupin *et al.* and Tamain *et al.*, where a blueshift in the 475 nm peak is typically observed in acidic plutonium solutions to 457–458 nm, which both sources claim is indicative of plutonium complexation.[24,42] Such observations further suggest that absorption spectroscopy is a powerful handle for monitoring oligomer formation and stability.

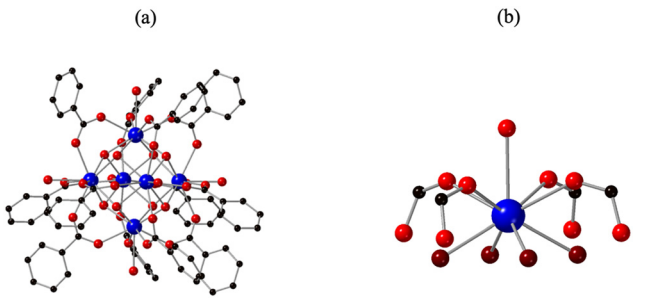

Fig. 1 Illustration of (a) **Th$_6$** cluster and (b) the local coordination environment about the Th metal centers. Thorium and carbon are shown in blue and black respectively. Oxygen atoms from water and the benzoate ligands are shown in red, and μ_3-oxygens in maroon. Hydrogen atoms and disorder have been omitted for clarity.

Vibrational spectroscopy

The vibrational spectra of **Th$_6$**, **U$_6$**, **Np$_6$**, and **Pu$_6$** were collected to further examine how the actinide contraction manifests in spectroscopic properties. The IR spectra of the

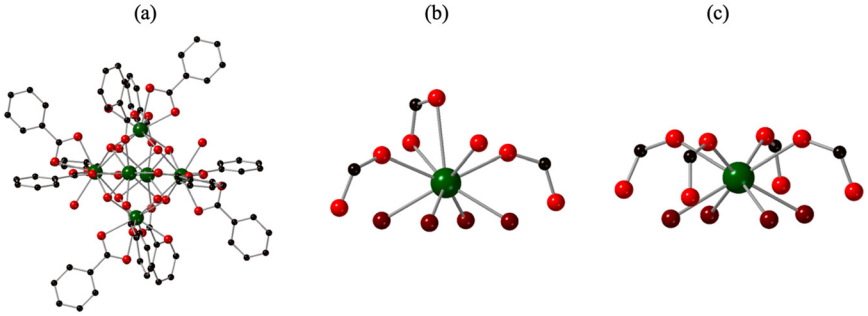

Fig. 2 Illustration of (a) $U_6/Np_6/Pu_6$ cluster, (b) the local coordination environment about the 9-coordinate metal centers, and (c) the local coordination environment about the 8-coordinate metal centers. Uranium/neptunium/plutonium and carbon are shown in green and black respectively. Oxygen, water, and benzoate oxygens are shown in red, and μ_3-oxygens are shown in maroon. Hydrogen atoms and disorder have been omitted for clarity.

Table 2 Summary of coordination number and An–O and An–An distances for Th_6, U_6, Np_6,[a] and Pu_6

Compound	An coordination number	An–μ_3O (Å)	An–μ_3OH (Å)	An–$O_{benzoate}$ (Å)	An–O_{water} (Å)	An–An distance (Å)
Th_6	9	2.31(1)	2.51(1)	2.49(2)	2.70(1)	3.944(3)
U_6	8/9	2.25(4)	2.462(37)	2.458(10)	2.46(1)	3.84(5)
Np_6	—	2.22(12)	2.41(15)	N/A	N/A	3.81(5)
Pu_6	8/9	2.23(3)	2.44(4)	2.45(1)	2.41(3)	3.80(5)

[a] Only a preliminary refinement of Np_6 was obtained, therefore average An–$O_{benzoate}$ and An–O_{water} distances are not provided.

compounds are shown in Fig. 6 and a complete listing of the observed bands is provided in the ESI.† As expected, the spectra are largely dominated by vibrational modes of the benzoate ligands. The medium intensity peak centered at 1390 cm^{-1} is the result of a C–C aromatic stretch, the split bands between 1530–1690 cm^{-1} are a result of a conjugated C=O stretch, and the broad peak above 3000 cm^{-1} is indicative of aromatic C–H stretches.[58] Notably, these stretches are all present within the spectrum of Np_6, further suggesting that benzoates do in fact decorate the cluster. Also, the sharp peak above 3600 cm^{-1} is attributed to the μ_3-OH stretch.[59] This peak is evident for Th_6, however is less

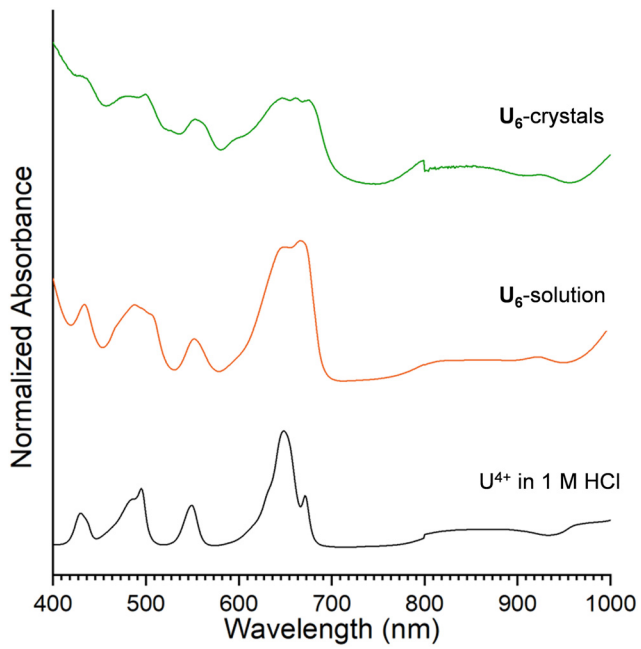

Fig. 3 UV-vis–NIR absorption spectra of UCl_4 in 1 M HCl (black), U_6 reaction solution (orange), and U_6 crystals (green).

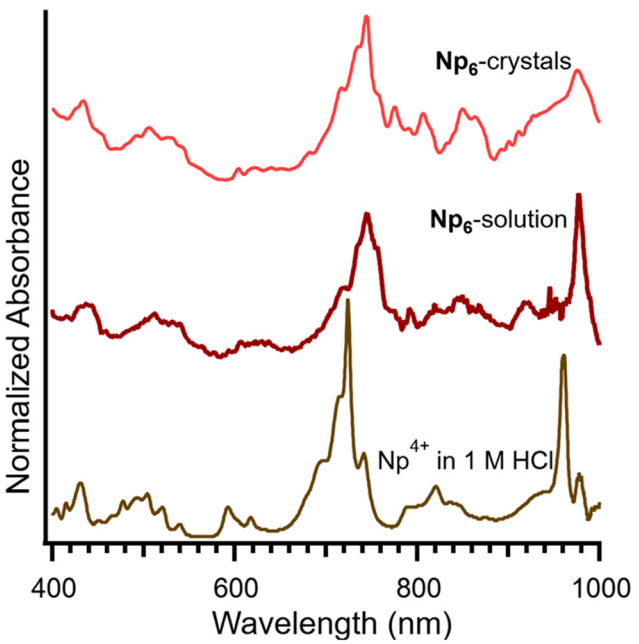

Fig. 4 UV-vis–NIR absorption spectra of Np^{4+} in 1 M HCl (brown), Np_6-solution (dark red), and Np_6-crystals (red).

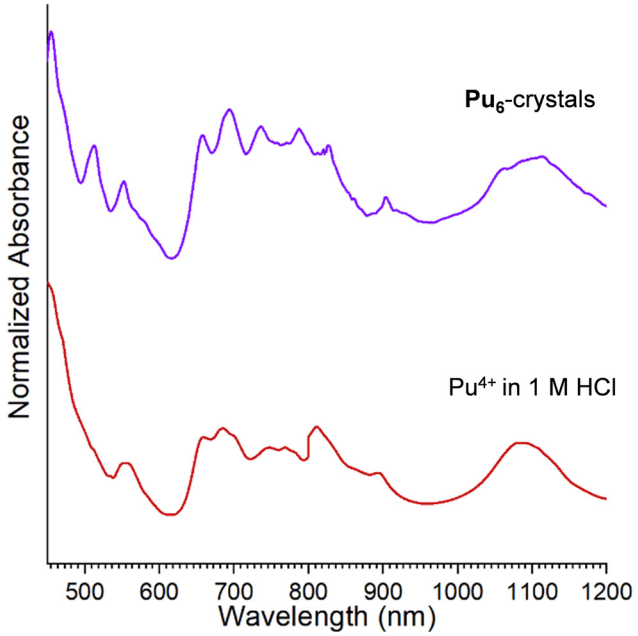

Fig. 5 UV-vis–NIR absorption spectra of Pu^{4+} in 1 M HCl (red) and Pu_6-crystals (purple).

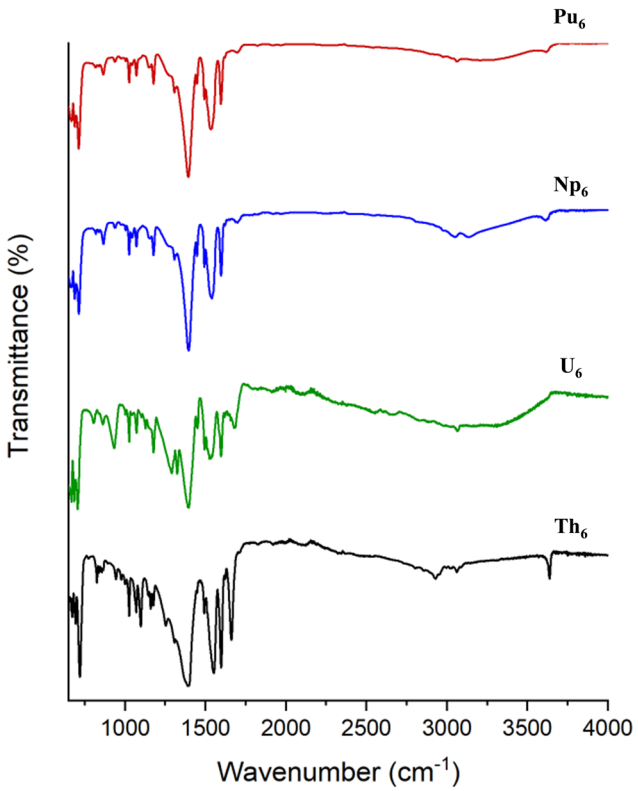

Fig. 6 Infrared spectra of Th_6 (black), U_6 (green), Np_6 (blue), and Pu_6 (red).

intense for Pu_6 and Np_6 and not present for U_6. This is likely the result of the overall lower IR intensity for U_6 relative to the other phases. Somewhat surprisingly, no peaks within the IR appear to trend with differences in bond lengths across the series. This is likely due to the fact that An–O are likely low-frequency vibrations outside the range of the collected spectra.[28]

The Raman spectra of each of the clusters agree with each other and exhibit bands consistent with the decorating benzoate ligand (Fig. S9†). Specifically, peaks observed at ~835 cm^{-1} (COO– in plane scissoring), 1003 cm^{-1} (aromatic ring stretch), and 1604 cm^{-1} (aromatic ring stretch) are all attributed to benzoate.[60] As for the expected An–O stretches, based on the mass of the actinide ion relative to the rest of the atoms in the cluster, they would most likely appear within the low frequency region ($\leq$500 cm^{-1}).[59] Unfortunately, like the IR spectra, stretches in this portion of the spectra are low resolution and therefore, their assignment cannot be made with certainty.

Conclusions

A series of four An^{4+}–oxo hexamers (An = Th, U, Np, Pu) is reported. While such clusters have been previously described, this work examines the formation of an analogous series of hexamers across the early actinides, Th–Pu, such that the effects of increasing charge density, and hence metal ion acidity, on synthesis could be examined. The decreased Brønsted acidity of Th relative to the later actinides, U–Pu, is evidenced in this work by observation of a non-hydrolyzed Th chain, $[Th(Bz)_4]_n$ and the inability to translate the synthetic conditions used to isolate U_6, Np_6, and Pu_6. Further, structural characterization of the phases through single crystal X-ray diffraction show that U and Pu adopt the same cluster core, while Th differs in the number and connectivity of the decorating ligands; these differences reflect trends in periodicity that arise from the actinide contraction. Additionally, investigations into the UV-vis–NIR absorption behavior of these compounds and the solutions from which they crystallize lend insight into spectroscopic handles that can be used for the identification of these species in both in solution and the solid state.

Experimental methods

Synthetic procedure

CAUTION: thorium-232 ($t_{1/2}$ = 1.42 × $10^{10}y$), uranium-238 ($t_{1/2}$ = 4.5 × $10^{9}y$), neptunium-237 ($t_{1/2}$ = 2.1 × $10^{6}y$), and plutonium-239 ($t_{1/2}$ = 2.4 × $10^{4}y$) are hazardous α and γ emitting radionuclides. Bulk transuranium samples pose a serious health risk and must be studied in a facility designed and designated for the handling of highly radioactive and toxic heavy metals. Bulk material manipulations were conducted in a negative pressure radiological glovebox, while subsamples were handled within radiological fume hoods.

Thorium chloride ($ThCl_4$) (International Bioanalytical Industries, Inc.), uranyl oxide (UO_3) (International Bioanalytical Industries, Inc.), hexachloropropene (Sigma Aldrich), benzoic acid (BA, Fisher Scientific), hydroxylamine hydrochloride (Fisher Scientific), and ethanol (EtOH, Fisher

Scientific) were all used as received from the commercial suppliers. Dimethylformamide (DMF, Fisher Scientific) was dried overnight on molecular sieves (Fisher Scientific) prior to use. Uranium chloride (UCl_4) was prepared from UO_3 in hexachloropropene following the approach designed by Patel *et al.*[61] Preparation of the Np^{4+} and Pu^{4+} stock solutions is described below. Nanopure water (≤0.05 μS; Millipore USA) was used in all reactions.

The compound **Th$_6$**, $[Th_6O_4(OH)_4(C_7H_5O_2)_{12}(H_2O)_6]$, was prepared using an approach adapted from that described for Th–UiO-66, $[Th_6O_4(OH)_4(C_8H_6O_4)_{12}]$.[54] $ThCl_4$ (0.010 g, 0.0267 mmol) and 300 μL of a 0.328 M solution of benzoic acid in DMF (0.012 g, 0.0984 mmol) were added to a 23 mL Teflon cup. The Teflon cup was placed in a 23-mL Parr acid digestion vessel and heated statically at 130 °C for 24 hours. The vessel was removed from the oven and allowed to cool to room temperature prior to opening. Slow evaporation of the resulting colorless solution under ambient conditions in a 4 dram shell vial over 24 hours yielded colorless block-like crystals. Yield: 44% based on Th^{4+}.

The compound **U$_6$**, $[U_6O_4(OH)_4(C_7H_5O_2)_{12}(H_2O)_4]\cdot 2(C_2H_6O)\cdot 2.5(H_2O)$, was synthesized at room temperature in a nitrogen filled glovebox. The latter was used to limit oxidation of uranium. The starting material, UCl_4 (0.075 g, 0.197 mmol), was dissolved in H_2O (1 mL) in a 4 dram shell vial. In a separate vial, BA (0.048 g, 0.393 mmol) was dissolved in EtOH (1 mL). The organic and aqueous solutions were combined, and the resulting solution was left to slowly evaporate for 12 hours. The initial pH of the solution was 1.13. Green crystals precipitated over 24 hours. Yield: 48% based on U^{4+}.

The compound **Np$_6$**, $[Np_6O_4(OH)_4(C_7H_5O_2)_{12}(H_2O)_4]\cdot x(C_2H_6O)\cdot y(H_2O)$ was synthesized using a similar approach as **U$_6$**. A Np^{4+} solution was prepared *via* chemical reduction of a Np^{5+}/HCl solution (0.702 mL, 30 mM solution, 0.0211 mmol of ^{237}Np) with hydroxylamine hydrochloride (21 mg, 0.757 mmol). The oxidation state of Np was confirmed *via* UV-vis absorption spectroscopy (Fig. 4). Following the reduction to Np^{4+}, the solution was evaporated to near dryness and then reconstituted with 0.500 mL of water. Benzoic acid (32 mg, 0.262 mmol) was dissolved in EtOH (0.5 mL), and the resulting solution was added to the Np^{4+} stock solution; the pH was 0.12. The reaction mixture was diluted with EtOH (1.250 mL); the pH of the resulting solution was 2.28. The solution was left to evaporate and pale pink crystals precipitated over 24 hours. The crystals diffracted poorly; however, both the unit cell and a preliminary refinement of **Np$_6$** are consistent with a benzoate decorated hexamer. Powder X-ray diffraction (PXRD) further confirmed that **Np$_6$** was representative of the bulk precipitate (Fig. S8†).

The compound **Pu$_6$**, $[Pu_6O_4(OH)_4(C_7H_5O_2)_{12}(H_2O)_4]\cdot m(C_2H_6O)\cdot n(H_2O)$, was synthesized following the same general synthetic approach as that described for **U$_6$** and **Np$_6$**. A Pu^{4+} stock solution was prepared by heating ^{239}Pu (36 mg) in 6 M HCl to near dryness. This resulting residue was then redissolved in 2.4 mL of 0.5 M HCl (total concentration: 18.67 mg mL^{-1}). A solution of BA (9.09 mg, 0.0744 mmol) in 800 μL of a 1 : 1 H_2O/EtOH mixture was added to a Pu^{4+}/HCl stock solution (80.0 μL, 1.5 mg, 0.00628 mmol of ^{239}Pu). The initial pH was 0.6. The pH of the solution was adjusted to 1.0 using concentrated (50% wt/wt) NaOH. The solution was then slowly evaporated over 72 hours, after which red crystals and clear acicular needle-like crystals consistent with recrystallized BA were observed.

Powder X-ray diffraction

Powder X-ray diffraction data were collected for **Th$_6$**, **U$_6$**, and **Np$_6$** using a Rigaku Ultima IV diffractometer (Cu K = 1.524 Å, 2 = 3–40°). The **Np$_6$** compound was placed on a zero-background plate within a Bruker sample holder and contained using a Kapton® film.[62] Calculated diffraction patterns were generated using CIFs of **Th$_6$**, **U$_6$**, and **Np$_6$** and were compared to the experimental patterns. Agreement between the calculated and experimental patterns suggest that the crystals used for structure determination were representative of the bulk reaction product.

Vibrational spectroscopy

Raman spectra of **Th$_6$** and **U$_6$** were collected on single crystals using an HORIBA LabRAM HR Evolution Raman spectrometer equipped with a 532 nm laser. Spectra were collected at room temperature from 100–3200 cm^{-1}. Raman spectra of **Np$_6$** and **Pu$_6$** were collected on single crystals using a Renishaw inVia™ Raman spectrophotometer equipped with a 532 nm and 785 nm laser, respectively. Data were collected at room temperature from 100–3200 cm^{-1}. Infrared spectra for **Th$_6$** and **U$_6$** were collected using an Agilent Cary 630 FTIR. Single crystals were handpicked for measurement and spectra were collected from 650–4000 cm^{-1}. Infrared spectra for **Np$_6$** and **Pu$_6$** were collected using a Bruker Lumos FTIR spectrophotometer equipped with an attenuated total reflection accessory. Spectra were collected from 600–4000 cm^{-1} and data were processed using the OPUS V.7.2 software.

Optical UV-vis–NIR absorption spectroscopy

The solid-state UV-vis–NIR optical absorption spectrum was collected for **U$_6$** on an Agilent Cary 5000 UV-vis–NIR spectrophotometer. The sample was prepared by grinding individual crystals into dry KBr (Fisher Scientific) and placing the mixture into a solid-state sample holder. Spectra were collected from 200–1000 nm. The UV-vis–NIR absorption data for **Np$_6$** and **Pu$_6$** were collected on single crystals using a Craic solid-state UV-vis–NIR microscope spectrophotometer due to the limited yield. Crystals were transferred to a glass slide that was covered with a glass coverslip and sealed with epoxy. Spectra were collected from 200–1000 nm.

Solution-state data for **U$_6$** and other uranium-based solutions were collected on an Agilent Cary 5000 UV-vis–NIR spectrophotometer. Samples were placed in a quartz cuvette and spectra were collected from 200–1000 nm. Solution-state data for **Np$_6$**, **Pu$_6$**, as well as neptunium and plutonium-

based solutions, were collected using a Mikropack DH-2000-BALL deuterium and halogen light source coupled to an Ocean Optics Flame detector. Scattered light was collected with a fiber-optic cable. Data were then processed using OceanView spectroscopy software (V.2.0.8.).

Structure determination

Single crystals of **Th_6**, and **U_6** were selected from the bulk reaction product, mounted on MiTeGen micromounts in mineral oil, and placed on a Bruker D8 QUEST diffractometer equipped with a Photon 100 detector and a Mo IμS source (K = 0.71073 Å). Crystals of **Np_6** and **Pu_6** were mounted and super glued to MiTeGen micromounts, then covered with a heat-shrinkable sheath that was glued to the mount for secondary containment.[62] The single-crystal diffraction data were collected on a Bruker D8 Venture diffractometer equipped with a CMOS detector and a Mo IS source (K = 0.71073 Å). For all samples, data were reduced using SAINT and absorption corrections were applied using SADABS, both within the APEX III software.[63–65] The structure solutions were all performed using intrinsic phasing method and structure refinements were conducted using the ShelXle software.[66,67] It is important to note for **Np_6**, only a preliminary data collection and refinement was possible due to poor crystal quality and hence limited diffraction. As such, only unit cell parameters are provided. Further details of the refinement of **Th_6**, **U_6**, and **Pu_6** are provided in the ESI.†

Data availability

Data supporting the results presented in this manuscript including refinement details, thermal ellipsoid plots, powder X-ray diffraction patterns, and Raman spectra are provided as ESI.† Accession codes CCDC 2387949–2387951 contain the ESI† crystallographic data for this paper.

Author contributions

Please use **https://credit.niso.org/**, we have been asked by reviewers to use this method to acknowledge the contribution of each of the authors.

All authors have approved the final version of this manuscript. All authors contributed equally to this work. CRediT author statement. TLM: conceptualization, methodology, validation, formal analysis, investigation, writing, visualization. NAV: conceptualization, methodology, investigation. RGS: methodology, supervision. JESS: investigation. JAB: formal analysis. AA: methodology, formal analysis, investigation, resources, writing, supervision. KEK: conceptualization, methodology, formal analysis, resources, writing, and supervision.

Conflicts of interest

There are no conflicts to declare.

Acknowledgements

Synthesis and characterization of the thorium and uranium compounds were performed at Georgetown University, under the support of the U.S. Department of Energy, Office of Science, Office of Basic Energy Sciences, Early Career Research Program under Award DE-SC0019190. Both TLM and KEK were supported by this award. The neptunium and plutonium work was conducted at Pacific Northwest National Laboratory by TLM, RGS, and AA. TLM was supported under award DE-SC0019190. The funding mechanism for work performed by TLM and AA at PNNL was the Laboratory Directed Research and Development program at Pacific Northwest National Laboratory, a multiprogram national laboratory operated by Battelle for the Department of Energy. AA is grateful for support from the Linus Pauling Distinguished Postdoctoral Fellowship. RGS was supported by the U.S. Department of Energy, Office of Science, Office of Basic Energy Sciences, Division of Chemical Sciences, Geosciences and Biosciences, Heavy Element Chemistry program, under Award FWP 73200. The authors thank Ashley Hastings for providing insight into synthetic techniques which led to the successful isolation of the Th compound and Lulio Sanz for assistance in collecting solid-state UV-vis absorption data of **U_6**.

References

1 G. Choppin, *J. Radioanal. Nucl. Chem.*, 2007, **273**, 695–703.
2 K. E. Knope and L. Soderholm, *Chem. Rev.*, 2013, **113**, 944–994.
3 T. Loiseau, I. Mihalcea, N. Henry and C. Volkringer, *Coord. Chem. Rev.*, 2014, **266–267**, 69–109.
4 K. E. Knope and L. Soderholm, *Inorg. Chem.*, 2013, **52**, 6770–6772.
5 V. Neck and J. I. Kim, *Radiochim. Acta*, 2001, **89**, 1–16.
6 W. Küchle, M. Dolg and H. Stoll, *J. Phys. Chem. A*, 1997, **101**, 7128–7133.
7 A. P. Novikov, S. N. Kalmykov, S. Utsunomiya, R. C. Ewing, F. Horreard, A. Merkulov, S. B. Clark, V. V. Tkachev and B. F. Myasoedov, *Science*, 2006, **314**, 638–641.
8 A. B. Kersting, *Inorg. Chem.*, 2013, **52**, 3533–3546.
9 K. Maher, J. R. Bargar and G. E. Brown Jr, *Inorg. Chem.*, 2013, **52**, 3510–3532.
10 L. S. Natrajan, A. N. Swinburne, M. B. Andrews, S. Randall and S. L. Heath, *Coord. Chem. Rev.*, 2014, **266–267**, 171–193.
11 G. L. Johnson and L. M. Toth, *Plutonium (IV) and thorium (IV) hydrous polymer chemistry. [Conversion of hydrolye-bridged polymer links to oxygen-bridged linkages]*, Oak Ridge National Lab. (ORNL), Oak Ridge, TN (United States), 1978.
12 I. Colliard, J. C. Brown and M. Nyman, *Inorg. Chem.*, 2022, **62**, 1891–1900.
13 R. Faizova, F. Fadaei-Tirani, R. Bernier-Latmani and M. Mazzanti, *Am. Ethnol.*, 2020, **132**, 6822–6825.
14 D. Zhou, Y. Yang, Z. Weng, J. Wang, Y. Yan, L. Cheng, Y. Fan, L. Chen, H. Zhang and L. Chen, *Inorg. Chem.*, 2024, **63**, 14278–14283.

15 G. E. Sigmon and A. E. Hixon, *Chem. – Eur. J.*, 2019, **25**, 2463–2466.
16 N. P. Martin, C. Volkringer, P. Roussel, J. März, C. Hennig, T. Loiseau and A. Ikeda-Ohno, *Chem. Commun.*, 2018, **54**, 10060–10063.
17 N. P. Martin, C. Volkringer, N. Henry, X. Trivelli, G. Stoclet, A. Ikeda-Ohno and T. Loiseau, *Chem. Sci.*, 2018, **9**, 5021–5032.
18 C. Falaise, C. Volkringer, J.-F. Vigier, A. Beaurain, P. Roussel, P. Rabu and T. Loiseau, *J. Am. Chem. Soc.*, 2013, **135**, 15678–15681.
19 L. Soderholm, P. M. Almond, S. Skanthakumar, R. E. Wilson and P. C. Burns, *Angew. Chem., Int. Ed.*, 2008, **47**, 298–302.
20 D. Ray, J. Xie, J. White, G. E. Sigmon, L. Gagliardi and A. E. Hixon, *Chem. – Eur. J.*, 2020, **26**, 8115–8120.
21 R. E. Wilson, S. Skanthakumar, G. Sigmon, P. C. Burns and L. Soderholm, *Inorg. Chem.*, 2007, **46**, 2368–2372.
22 C. Tamain, T. Dumas, D. Guillaumont, C. Hennig and P. Guilbaud, *Eur. J. Inorg. Chem.*, 2016, **2016**, 3536–3540.
23 K. Takao, S. Takao, A. C. Scheinost, G. Bernhard and C. Hennig, *Inorg. Chem.*, 2012, **51**, 1336–1344.
24 G. Chupin, C. Tamain, T. Dumas, P. L. Solari, P. Moisy and D. Guillaumont, *Inorg. Chem.*, 2022, **61**, 4806–4817.
25 I. Colliard, G. Morrison, H.-C. zur Loye and M. Nyman, *J. Am. Chem. Soc.*, 2020, **142**, 9039–9047.
26 S. T. Tsantis, D. I. Tzimopoulos, M. Holynska and S. P. Perlepes, *Int. J. Mol. Sci.*, 2020, **21**, 555.
27 Y.-J. Hu, K. E. Knope, S. Skanthakumar and L. Soderholm, *Eur. J. Inorg. Chem.*, 2013, **2013**, 4159–4163.
28 K. E. Knope, M. Vasiliu, D. A. Dixon and L. Soderholm, *Inorg. Chem.*, 2012, **51**, 4239–4249.
29 C. Falaise, K. Kozma and M. Nyman, *Chem. – Eur. J.*, 2018, **24**, 14226–14232.
30 L. Chatelain, R. Faizova, F. Fadaei-Tirani, J. Pécaut and M. Mazzanti, *Angew. Chem., Int. Ed.*, 2019, **58**, 3021–3026.
31 Z.-J. Li, S. Guo, H. Lu, Y. Xu, Z. Yue, L. Weng, X. Guo, J. Lin and J.-Q. Wang, *Inorg. Chem. Front.*, 2020, **7**, 260–269.
32 P. Woidy and F. Kraus, *Z. Anorg. Allg. Chem.*, 2014, **640**, 1547–1550.
33 C. Falaise, C. Volkringer, C. Hennig and T. Loiseau, *Chem. – Eur. J.*, 2015, **21**, 16654–16664.
34 Z. Yue, X. Guo, M.-L. Feng, Y.-J. Lin, Y. Ju, X. Lin, Z.-H. Zhang, X. Guo, J. Lin and Y.-Y. Huang, *Inorg. Chem.*, 2020, **59**, 2348–2357.
35 S. T. Tsantis, A. Lagou-Rekka, K. F. Konidaris, C. P. Raptopoulou, V. Bekiari, V. Psycharis and S. P. Perlepes, *Dalton Trans.*, 2019, **48**, 15668–15678.
36 N. E. Travia, B. L. Scott and J. L. Kiplinger, *Chem. – Eur. J.*, 2014, **20**, 16846–16852.
37 K. E. Knope, S. Skanthakumar and L. Soderholm, *Inorg. Chem.*, 2015, **54**, 10192–10196.
38 J. Lin, M. Qie, L. Zhang, X. Wang, Y. Lin, W. Liu, H. Bao and J. Wang, *Inorg. Chem.*, 2017, **56**, 14198–14205.
39 X.-Y. Qian, T.-H. Zhou and J.-G. Mao, *Dalton Trans.*, 2015, **44**, 13573–13580.
40 D. K. Unruh, J. de Groot, M. Fairley, A. Libo, S. Miller and T. Z. Forbes, *Inorg. Chem.*, 2015, **54**, 1395–1404.
41 S. Fichter, T. Radoske and A. Ikeda-Ohno, *Acta Crystallogr., Sect. E:Crystallogr. Commun.*, 2021, **77**, 847–852.
42 C. Tamain, T. Dumas, C. Hennig and P. Guilbaud, *Chem. – Eur. J.*, 2017, **23**, 6864–6875.
43 L. M. Mokry, N. S. Dean and C. J. Carrano, *Angew. Chem., Int. Ed. Engl.*, 1996, **35**, 1497–1498.
44 N. A. Vanagas, J. N. Wacker, C. L. Rom, E. N. Glass, I. Colliard, Y. Qiao, J. A. Bertke, E. Van Keuren, E. J. Schelter, M. Nyman and K. E. Knope, *Inorg. Chem.*, 2018, **57**, 7259–7269.
45 C. Falaise, H. A. Neal and M. Nyman, *Inorg. Chem.*, 2017, **56**, 6591–6598.
46 N. A. Vanagas, R. F. Higgins, J. N. Wacker, D. R. C. Asuigui, E. Warzecha, S. A. Kozimor, S. L. Stoll, E. J. Schelter, J. A. Bertke and K. E. Knope, *Chem. – Eur. J.*, 2020, **26**, 5872–5886.
47 I. Colliard, C. Falaise and M. Nyman, *Inorg. Chem.*, 2020, **59**, 17049–17057.
48 X. Kong, X. Liao, Z. Huang, L. Mei, H. Wang, K. Hu and W. Shi, *Chin. Chem. Lett.*, 2024, **35**, 109642.
49 C. Falaise, C. Volkringer, J.-F. Vigier, N. Henry, A. Beaurain and T. Loiseau, *Chem. – Eur. J.*, 2013, **19**, 5324–5331.
50 N. P. Martin, J. März, H. Feuchter, S. Duval, P. Roussel, N. Henry, A. Ikeda-Ohno, T. Loiseau and C. Volkringer, *Chem. Commun.*, 2018, **54**, 6979–6982.
51 M. Rand, J. Fuger, I. Grenthe, V. Neck and D. Rai, Chemical Thermodynamics of Thorium, *Chemical Thermodynamics*, OECD Publishing, Paris, 2008.
52 I. Grenthe, X. Gaona, L. Rao, A. Plyasunov, W. Runde, B. Grambow, R. Konings, A. Smith, E. Moore and M.-E. Ragoussi, Second update on the chemical thermodynamics of uranium, neptunium, plutonium, americium and technetium, *Chemical thermodynamics*, Organisation for Economic Co-Operation and Development, 2020, vol. 14.
53 C. Falaise, C. Volkringer and T. Loiseau, *Inorg. Chem. Commun.*, 2014, **39**, 26–30.
54 C. Falaise, J.-S. Charles, C. Volkringer and T. Loiseau, *Inorg. Chem.*, 2015, **54**, 2235–2242.
55 D. Cohen and W. T. Carnall, *J. Phys. Chem.*, 1960, **64**, 1933–1936.
56 J. C. Hindman, L. B. Magnusson and T. J. LaChapelle, *J. Am. Chem. Soc.*, 1949, **71**, 687–693.
57 M. H. Lee, Y. J. Park and W. H. Kim, *J. Radioanal. Nucl. Chem.*, 2007, **273**, 375–382.
58 M. Kumar, R. Bala, V. S. Gondil, S. K. Pandey, S. Chhibber, D. V. S. Jain, R. K. Sharma and N. Wangoo, *J. Mater. Sci.*, 2017, **52**, 8568–8575.
59 A. M. Hastings, D. Ray, W. Jeong, L. Gagliardi, O. K. Farha and A. E. Hixon, *J. Am. Chem. Soc.*, 2020, **142**, 9363–9371.
60 W. Xi and A. J. Haes, *J. Chem. Phys.*, 2020, **153**, 184707.
61 D. Patel, A. J. Wooles, E. Hashem, H. Omorodion, R. J. Baker and S. T. Liddle, *New J. Chem.*, 2015, **39**, 7559–7562.
62 A. Arteaga, A. D. Nicholas, L. C. Ducati, J. Autschbach and R. G. Surbella III, *Inorg. Chem.*, 2023, **62**, 4814–4822.
63 *APEX2, version 2010.7*, Bruker AXS Inc., Madison, WI, 2010.
64 *SAINT*, Bruker AXS Inc., Madison, WI, 2007.
65 *SADABS*, Bruker AXS Inc., Madison, WI, 2008.

66 C. B. Hübschle, G. M. Sheldrick and B. Dittrich, *J. Appl. Crystallogr.*, 2011, **44**, 1281–1284.

67 G. M. Sheldrick, *Acta Crystallogr., Sect. C:Struct. Chem.*, 2015, **71**, 3–8.